Journal of Peptide Science
J. Peptide Sci. **9**: 156–169 (2003)
Published online in Wiley InterScience (www.interscience.wiley.com). DOI: 10.1002/psc.442

JOURNAL OF PEPTIDE SCIENCE

The Role of Segment 32–47 of Cholecystokinin Receptor Type A in CCK8 Binding: Synthesis, Nuclear Magnetic Resonance, Circular Dichroism and Fluorescence Studies

STEFANIA DE LUCA,[a] RAFFAELE RAGONE,[b] CHIARA BRACCO,[c] GIUSEPPE DIGILIO,[c] DIEGO TESAURO,[a] MICHELE SAVIANO,[a] CARLO PEDONE[a] and GIANCARLO MORELLI[a]*

[a] Centro Interuniversitario di Ricerca sui Peptidi Bioattivi & Istituto di Biostrutture e Bioimmagini, CNR, 80134 Napoli, Italy
[b] Dipartimento di Biochimica e Biofisica, Seconda Università di Napoli, 80138 Napoli, Italy
[c] Bioindustry Park del Canavese, 10010 Colleretto Giacosa (TO), Italy

Received 8 July 2002
Accepted 16 September 2002

Abstract: The segment 32–47 of the *N*-terminal extracellular domain of the type A cholecystokinin receptor, CCK_A-R(32–47), was synthesized and structurally characterized in a membrane mimicking environment by CD, NMR and molecular dynamics calculations. The region of CCK_A-R(32–47) encompassing residues 39–46 adopted a well-defined secondary structure in the presence of DPC micelles, whereas the conformation of the *N*-terminal region (segment 32–37) could not be uniquely defined by the NOE derived distance constraints because of local flexibility. The conformation of the binding domain of CCK_A-R(32–47) was different from that found for the intact *N*-terminal receptor tail, CCK_A-R(1–47). To assess whether CCK_A-R(32–47) was still able to bind the nonsulfated cholecystokinin *C*-terminal octapeptide, CCK8, a series of titrations was carried out in SDS and DPC micelles, and the binding interaction was followed by fluorescence spectroscopy. These titrations gave no evidence for complex formation, whereas a high binding affinity was found between CCK_A-R(1–47) and CCK8. The different affinities for the ligand shown by CCK_A-R(32–47) and CCK_A-R(1–47) were paralleled by different interaction modes between the receptor segments and the micelles. The interaction of CCK_A-R(32–47) with DPC micelles was much weaker than that of CCK_A-R(1–47), because the former receptor segment lacks proper stabilizing contacts with the micelle surface. In the case of SDS micelles CCK_A-R(32–47) was found to form non-micellar adducts with the detergent that prevented the onset of a functionally significant interaction between the receptor segment and the micelle. It is concluded that tertiary structure interactions brought about by the 1–31 segment play a key role in the stabilization of the membrane bound, biologically active conformation of the *N*-terminal extracellular tail of the CCK_A receptor.

Keywords: CCK_A receptor; CCK8 binding; fluorescence; NMR

Abbreviations: Boc, *tert*-butoxycarbonyl; tBu, *tert*-butyl; CCK, cholecystokinin; CCK8, *C*-terminal octapeptide of cholecystokinin; CD, circular dichroism; c.m.c., critical micellar concentration; DIPEA, diisopropylethylamine; DMF, *N*,*N*-dimethylformamide; DPC, dodecylphosphatidylcholine; DQF-COSY, double quantum filtered correlation spectroscopy; 5-DS, 5-doxylstearate; EDC, 1-[3-(dimethylamino)propyl]-3-ethyl carbodiimide; Fmoc, 9-fluorenylmethoxycarbonyl; GPCR, G-protein coupled receptor; HOBt, 1-hydroxy-1,2,3-benzotriazole; NOESY, nuclear Overhauser effect spectroscopy; Pbf, 2,2,4,6,7-pentamethyl-dihydrobenzofuran-5-sulfonyl; PFG, pulse field gradient; PyBop, benzotriazol-1-yl-oxy-tris-pyrrolidino phosphonium; RMSD, root mean square deviation; SDS, sodium dodecylsulfate; TAD, torsion angle dynamics; TFA, trifluoroacetic acid; TMS, tetramethylsilane; TOCSY, total correlation spectroscopy; TPPI, time proportional phase increment; Trt, trityl.

*Correspondence to: Dr Giancarlo Morelli, Centro Interuniversitario di Ricerca sui Peptidi Bioattivi, via Mezzocannone 6–8, 80134 Napoli, Italy; e-mail: morelli@chemistry.unina.it
Contract/grant sponsor: Italian MURST (PS Oncologia).
Contract/grant sponsor: Bracco Imaging SpA, Milan.

INTRODUCTION

CCK peptide hormones are specifically recognized by two distinct receptors (CCK_A-R and CCK_B-R) that belong to the GPCR superfamily. These receptors are very complex integral membrane proteins, which are constituted by seven transmembrane α-helix domains connected by extracellular and intracellular loops. The *N*-terminal tail extends towards the extracellular side, whereas the *C*-terminal tail protrudes towards the cytoplasmatic side. Although x-ray diffraction and theoretical methods have provided a model for the topological orientation of the seven transmembrane helices, little structural insight into the functional conformation of the extracellular loops and tail, which are responsible for molecular recognition, is currently available. The localization of the ligand binding domain within the intact CCK_A receptor has been achieved by photoaffinity cross-linking and mutagenesis studies, which pointed out the key role of the *N*-terminal tail and of the third extracellular loop [1–4]. Further high resolution structural studies have been carried out on simplified systems, where selected receptor fragments have been titrated with the *C*-terminal octapeptide of cholecystokinin, CCK8 [5,6]. The resulting complexes were characterized by NMR and extensive computer simulations. These studies provided molecular models for the interaction between CCK8 and the CCK_A-R(1–47) or CCK_A-R(329–357) segments (corresponding to the *N*-terminal tail and to the third extracellular loop, respectively) [5,6]. The CCK8/CCK_A-R(1–47) contact site was found to be located around residue Trp^{39} of CCK_A-R(1–47), as demonstrated by the detection of intermolecular NOEs between that residue and Tyr^{27}/Met^{28} of the CCK8 ligand. Furthermore, the ^{1}H-NMR signals of CCK_A-R(1–47) Trp^{39} were found to be specifically shifted upon titration of the receptor with the ligand [6]. It was therefore concluded that CCK8 forms specific interactions with the *N*-terminal extracellular tail of the CCK_A receptor. On this basis, we have recently determined the dissociation constant of the bimolecular complex CCK8/CCK_A-R(1–47) by fluorescence spectroscopy [7]. When the sulfated form of CCK8 was used as a ligand, an additional ligand/receptor contact site was detected, involving the Tyr sulfate moiety of CCK8 and residue Arg^{197} belonging to the second transmembrane loop (TM2) of CCK_A-R [2].

Besides the region around Trp^{39}, other residues in the CCK_A-R(1–47) sequence could be important for molecular recognition. Residues Cys^{18} and Cys^{29} are linked by a disulfide bridge that constitutes a major determinant of tertiary structure. The reduced form of CCK_A-R(1–47) spontaneously oxidizes to form an intramolecular disulfide bridge, indicating a conformational preference which brings the two Cys residues close to each other [6]. Reduction of the disulfide bonds in the closely related CCK_B receptor abolishes all affinity for the natural ligand [8], thus implying that the amino acid sequence comprising Cys^{18} and Cys^{29} plays a role in maintaining the active fold of the extracellular tail and in preserving the biological function of the entire CCK_A receptor. However, the contribution of the disulfide bridge (and, ultimately, of tertiary structure interactions) to the ligand binding affinity is still rather controversial. Recent biological studies demonstrated that truncation of the receptor to eliminate residues 1–30 had no detrimental effect on CCK binding, but the truncated receptor was found to be more sensitive to extracellular trypsin degradation than the wild type receptor. Thus, domain 1–30 has been proposed to play a protective role against extracellular trypsin damages [4].

To investigate on the role of tertiary structure interactions in the *N*-terminal tail of CCK_A receptor, we have synthesized the 32–47 segment, CCK_A-R(32–47). This hexadecapeptide was designed on the basis of the bimolecular complex between CCK_A-R(1–47) and CCK8 in such a way as to isolate the minimum molecular determinant which is involved in molecular recognition. The CCK_A-R(32–47) segment lacks the first part of the *N*-terminal extracellular domain (including the Cys residues), while it contains a few residues of the first transmembrane helix (TM1) of CCK_A receptor which are expected to interact with a membrane-like environment in much the same manner as CCK_A-R(1–47) does [6,7]. The presence of Trp^{39} in CCK_A-R(32–47) and Trp^{30} in CCK8 respectively should make it possible to monitor ligand-binding interactions by fluorescence measurements as previously described [7].

In this paper we report about the characterization of the CCK_A-R(32–47) peptide by NMR, CD and fluorescence techniques. We have performed NMR and molecular dynamics studies in DPC micelles to assess whether the CCK_A-R(32–47) segment retained a conformation able to interact with CCK8. In addition, we have carried out fluorescence and CD measurements in the presence of SDS or DPC either at submicellar and micellar concentrations in order to assess the binding affinity of this segment towards CCK8.

MATERIALS AND METHODS

Peptide Synthesis

The receptor fragment CCK_A-R(32–47), consisting of a sequence of 16 amino acids of the human CCK_A receptor, with free amino- and carboxy-termini, and the CCK8 peptide were obtained by solid-phase peptide synthesis, performed under standard conditions using the Fmoc strategy. The fully automated peptide synthesizers Shimadzu SPPS-8 (CCK8) and Milligen/Biosearch 9050 [CCK_A-R(32–47)] were used with a 0.100 mmol scale for both peptides. Double couplings were performed, in both cases by adding four equivalents of protected amino acids activated by PyBop [9] and EDC/HOBt [10] and eight equivalents of DIPEA in DMF; the stirring time was 60 min for each coupling. The protecting groups on amino acid side chains were: Trt for Gln; Pbf for Arg; tBu for Ser and Tyr; OtBu for Glu and Asp; Boc for Lys and Trp. For deprotection and cleavage the fully protected CCK8 peptide resin was treated with TFA containing triisopropylsilane (2.0%), ethanedithiole (2.5%) and water (1.5%), whereas the CCK_A-R(32–47) peptide resin was treated with TFA containing thioanisole (5.0%), phenol (5.0%), tri-isopropylsilane (1.0%), ethanedithiole (2.5%) and water (5.0%); both peptides were precipitated at 0 °C by adding diethyl ether dropwise. Purification of the crude mixtures was carried out by RP-HPLC.

Analytical RP-HPLC was carried out on a Shimadzu 10A-LC using a Phenomenex C_{18} column, 4.6×250 mm, eluted with an H_2O/0.1% TFA (A) and CH_3CN/0.1% TFA (B) linear gradient from 20% to 80% B over 45 min at 1 ml/min flow rate. Preparative RP-HPLC was carried out on a Waters Delta Prep 4000 equipped with an UV Lambda-Max 481 detector using a Vydac C_{18} column, 22×250 mm with the same eluants and gradient as used on the analytical scale. R_t(CCK8) = 25.2 min; R_t(CCK_A-R(32–47)) = 16.2 min. HPLC purity grade were 97% and 93%, respectively. Mass spectra carried out on MALDI-Tof Voyager-DE (PerSeptive Biosystems) confirmed the product identity: MW (CCK8): calcd. 1063.2; found 1062.0; MW CCK_A-R(32–47)) calcd. 1890.3; found 1889.6.

Absorption Spectroscopy

Concentrations of all solutions were measured by absorbance on a Jasco V-550 spectrophotometer using a molar absorptivity (ε_{280}) of 5630 and 6845 M^{-1} cm^{-1} for CCK_A-R(32–47) and CCK8, respectively. These values were calculated according to the Edelhoch method [11], by taking into account the contributions from Tyr and Trp present in the primary structure, which were reported to amount to 1215 and 5630 M^{-1} cm^{-1}, respectively [12]. Before measurements, all solutions were centrifuged, filtered and their limpidity was checked by absorbance at 325 nm, where absorption should be negligible.

NMR

DPC-d_{38} (98.96% atom D) was purchased from CDN Isotopes, whereas non-deuterated DPC was obtained from Avanti Polar Lipids. Typically, 1.50 mg of CCK_A-R(32–47) was dissolved into 600 µl of a freshly prepared micelle solution ([DPC-d_{38}] = 170 mM) in H_2O/D_2O 90% or in D_2O. The peptide concentration was 1.3 mM. The pH was adjusted to 6.5 ± 0.1 by adding small amounts of NaOH or HCl. When seeking intermolecular micelle/peptide NOEs, 10% of non-deuterated DPC was added to DPC-d_{38} in order to obtain a total DPC concentration of 170 mM. The titration of CCK_A-R(32–47) in DPC micelles with CCK8 was carried out by adding aliquots of 0.4 mg of the solid ligand to 600 µl of a solution containing 1.3 mM CCK_A-R(32–47) and DPC-d_{38}, and adjusting the pH to 6.5 if required.

The samples were transferred into 5 mm tubes for NMR analysis. NMR experiments were carried out on a Bruker Avance 600 MHz spectrometer operating at 14 T (corresponding to a resonance frequency of 600 MHz for the ^1H nucleus) equipped with a triple axis-PFG probe optimized for ^1H detection. Water suppression was achieved by means of the WATERGATE 3-9-19 pulse train [13,14] in the case of H_2O/D_2O 90% mixtures. Chemical shifts were referenced to an external solution (coaxial insert) containing 0.03% TMS in $CDCl_3$. 2D-TOCSY experiments [15] were carried out by means of a MLEV17 spin-lock pulse sequence [16] preceded by a 2.5 ms trim-pulse with a spin locking field strength of 10 KHz. The STATES-TPPI phase cycling was used to obtain complex data points in the t_1 dimension. Typically, the following instrumental settings were used for TOCSY experiments: spectral width 6900 Hz, 512 and 2048 complex data points in the t_1 and t_2 dimensions respectively, 32 to 64 scans per t_1 increment, relaxation delay 3 s, mixing time 100 ms. The data were apodized with a square cosine window function and zero filled to a matrix of size 1024×1024 prior to FT and baseline correction.

2D-NOESY experiments [17] were carried out by the standard pulse sequence with the STATES-TPPI phase cycling scheme with mixing times ranging from 100 to 350 ms. Typical instrumental settings included: spectral width 6900 Hz in both f_1 and f_2, 2048×512 data points in t_2 and t_1 respectively, 32 to 64 scans per t_1 increment, recycle delay 3 s. The data were apodized along both t_1 and t_2 dimensions with a square cosine window function and zero-filled to a symmetrical matrix of size 1024 x 1024 data points prior to FT and baseline correction.

2D-DQF-COSY experiments [18] were obtained in the phase sensitive mode by means of the TPPI method with the standard double quantum filtered pulse sequence coupled with a combination of PFG at the magic angle and selective water excitation to achieve optimal water suppression [19]. Typical instrumental settings included: spectral width 6600 Hz in f_1 and f_2, 4096×512 data points in t_2 and t_1, recycle delay 3 s, 64 scans per t_1 increment. The data were apodized with a square cosine window function and zero filled to a matrix of size 2048×1024 prior to FT and baseline correction.

Molecular Dynamics

All the calculations were carried out on a Silicon Graphics Octane workstation. The assignment of NMR signals and integration of NOE peaks were performed by means of the XEASY [20] software package. The assignment of ^{1}H-NMR resonances was carried out by the sequence-specific method [21], i.e. by iterative comparison of TOCSY, NOESY and DQF-COSY spectra. A number of ambiguities in the assignment due to severe signal overlap could be resolved by comparing experiments carried out at different temperatures. Peak volumes were obtained from NOESY spectra acquired with mixing times of 100–200 ms and converted into upper limit distance bounds by the CALIBA module in DYANA [22]. In order to take into account the effect of local motions on the intensity of the NOE signals, the peak volume-to-internuclear upper limit bound conversion was executed by classifying the NOEs into three different calibration classes and applying to each of them a different calibration function: (i) NOE peaks between backbone protons (amide protons, H^{α} and H^{β}) were converted with the function $V = A/d^6$; (ii) NOE peaks involving side-chain protons (except H^{β} and methyl groups) were calibrated with the function $V = B/d^4$; (iii) NOE peaks involving methyl groups were calibrated with the function $V = C/d^4$. Upper distance limits involving diastereotopic atom pairs without stereospecific assignment were modified in order to allow for both assignments by using the strategy described elsewhere [23].

The conformation of the molecule was optimized by means of molecular dynamics in the torsion angle space (TAD) coupled with simulated annealing. Such calculations were carried out by the program DYANA [22] (energy minimization by torsion angle dynamics and simulated annealing) and the obtained structures were analysed by means of MOLMOL [24] (molecular graphics). As many as 1000 conformers with all *trans* peptide bonds geometry and random values for all ϕ, ψ and χ dihedral angles were generated. Bond lengths and bond angles were kept fixed at their optimal values according to the ECEPP/2 [25] standard geometry. The initial random conformers were independently minimized by performing 100 conjugate gradient minimization steps including only distance constraints between atoms up to three residues far apart in the sequence. Hydrogen atoms were not considered explicitly for the check of steric overlap. One hundred more conjugate gradient minimization steps were carried out with the complete set of restraints. Then, each random conformer underwent 1000 TAD steps at an equilibration reference temperature of 9600 K with an initial time-step of 2 fs, followed by 4000 TAD steps with slow cooling close to zero temperature. The hydrogen atoms were then explicitly included into the check for steric overlap and 100 conjugate gradient minimization steps were performed, followed by 200 TAD steps at zero reference temperature. In the end, 1000 final conjugate gradient minimization steps were taken. Throughout these calculations the contribution to the target function due to the violation of upper limit distance constraints was measured according to a square potential function. The optimized conformers were ranked according to increasing residual target function values and accepted if such values were below the cutoff value of 0.3 Å^2 (the residual target function describes the consistency of a given structure with both geometric and steric constraints).

Circular Dichroism

Far-UV CD spectra were collected at room temperature on a Jasco J-715 spectropolarimeter using 1 cm quartz cells. Other experimental settings were: scan speed, 10 nm/min; sensitivity, 50 mdeg; time constant, 16 s; bandwidth, 3 nm. SDS titrations were carried out by adding small aliquots of a concentrated surfactant solution to a fixed volume of CCK_A-R(32–47) dissolved in 10 mM phosphate buffer, pH

7.2, and waiting for the achievement of an apparent equilibrium before measurements. Then, spectra were recorded, corrected for blank, and adjusted for dilution. The dichroic signal at 220 nm was used to follow SDS-induced secondary structure changes. Spectroscopic parameters were followed as a function of the total SDS concentration, best-fitted to sigmoidal curves by the program Scientist from MicroMath Software, San Diego (CA), and then normalized in terms of the maximal change observed.

Fluorescence

By analogy with what was previously observed for CCK_A-R(1–47) [7], the interaction between CCK_A-R(32–47) and CCK8 was presumed to modify Trp fluorescence. Thus, fluorescence spectra were recorded after each addition of small aliquots of concentrated CCK8 mother solution to a fixed volume of either CCK_A-R(32–47) or phosphate buffer in the presence of submicellar or micellar amounts of suitable surfactants. Either 8 mM SDS or 2 mM DPC were sufficient to ensure the presence of micellar aggregates. At the ionic strength of these experiments (10 mM phosphate buffer, pH 7.2), these concentrations are close to the respective c.m.c. in water (8.3 and 1.5 mM for SDS [26–28] and DPC [29], respectively). They are therefore noticeably higher than the actual c.m.c., because above the c.m.c. any ionic surfactant or detergent species is incorporated into micelles with an inverse ionic strength dependence [30,31]. To work in the range of fluorescence linearity the absorbance of solutions was always less than 0.1 at the excitation wavelength. Emission spectra were then recorded at room temperature using a Cary Eclipse fluorescence spectrophotometer with the excitation wavelength set at 295 nm to selectively excite Trp. Equal excitation and emission bandwidths were used throughout experiments, with a recording speed of 600 nm/min and a time constant of 0.1 s. Measurements were always performed after allowing solutions to stand until an apparent equilibrium was reached, as judged by the constancy of the fluorescence intensity. Final fluorescence intensities were always obtained after blank correction, adjustment for dilution, and subtraction of the separate contributions of CCK8 and CCK_A-R(32–47) from the total fluorescence. Using such a procedure, the fluorescence signal must either hyperbolically depart from 0 or remain unchanged, depending on its ability to detect binding interaction. SDS titration was carried out by adding small aliquots of a concentrated SDS solution to a fixed volume of peptide solution, and by monitoring the shift of the maximum emission wavelength, which is sensitive to overall structural changes. Spectroscopic parameters were followed as a function of the total SDS concentration, and best-fitted to sigmoidal curves as described for CD experiments.

RESULTS

NMR Structure of CCK_A-R(32–47) in DPC/Water

The assignment of the proton resonances of CCK_A-R(32–47) was achieved by means of the sequence specific method. The ^{1}H-NMR chemical shifts are reported in Table 1. In DPC micelles at 285 K each of residues Gln^{32}, Pro^{33} and Arg^{34} showed two sets of signals with relative intensity ratio of about 10 : 1, indicating the presence of different, slowly interconverting (on the NMR timescale) conformations at the *N*-terminus. At 298 K only one set of signals was observed, indicating that the timescale of the exchanging processes moved into the fast exchange limit. The differences in the conformations between the major and minor isomers are not due to *cis-trans* isomerism at the Xxx-Pro peptide bonds because Pro^{33} and Pro^{35} showed NOE correlations between their H^{δ} atoms and the H^{α} atom of the preceding residue both in the major and minor isomers. Thus, both isomers are endowed with a *trans* conformation of the Xxx-Pro peptide bonds. Also Pro^{41} invariantly showed NOE contacts typical of the *trans* conformation. More detailed insights into the conformational features of CCK_A-R(32–47) in the presence of DPC micelles could be obtained by means of restrained TAD and simulated annealing calculations. A series of 2D-NOESY spectra were acquired at 285 K and 298 K with mixing times ranging from 100 to 350 ms. At mixing times equal or shorter than 200 ms no significant spin diffusion effects were found. NOESY spectra acquired at 298 K with mixing times of 100 ms were initially used to derive the geometric constraints to be used for structure optimization. One thousand random conformations of the peptide were generated and independently energy minimized by constrained TAD and simulated annealing. An ensemble of 30 conformers endowed with the lowest residual target function values (e.g. showing the lowest constraint violations and the highest steric consistency) was then selected out of the bundle of 1000

Table 1 ^{1}H NMR Chemical Shifts of CCK_A-R(32–47) in DPC Micelle/Water Solution at 298 K and 285 K[a,b]

Residue	^{1}H atom	T = 298 K	T = 285 K
Gln 32	α-CH	4.31	4.27
	β-CH_2	2.11	2.11
	γ-CH_2	2.47	2.46
	ε-NH_2	7.64, 6.92	7.70, 6.97
Pro 33	α-CH	4.51	4.49
	β-CH_2	2.32, 1.87	2.31, 1.86
	γ-CH_2	2.01	2.00
	δ-CH_2	3.75, 3.61	3.74, 3.60
Arg 34	NH	8.53	8.63
	α-CH	4.61	4.58
	β-CH_2	1.86	1.83
	γ-CH_2	1.73	1.70
	δ-CH_2	3.21	3.19
Pro 35	α-CH	4.37	4.33
	β-CH_2	2.23, 1.88	2.24, 1.94
	γ-CH_2	2.00	2.00
	δ-CH_2	3.78, 3.62	3.77, 3.61
Ser 36	NH	8.31	8.41
	α-CH	4.36	4.34
	β-CH_2	3.90, 3.83	3.89, 3.82
Lys 37	NH	8.43	8.53
	α-CH	4.26	4.25
	β-CH_2	1.75	1.74
	γ-CH_2	1.40	1.39
	δ-CH_2	1.68	1.66
	ε-CH_2	2.98	2.94
Glu 38	NH	8.43	8.47
	α-CH	4.26	4.25
	β-CH_2	2.03, 1.89	2.23, 1.88
	γ-CH_2	2.24	2.02
Trp 39	NH	8.17	8.27
	α-CH	4.57	4.54
	β-CH_2	3.25	3.25
	1-NH	10.46	10.48
	2H	7.29	7.28
	4H	7.53	7.52
	5H	7.02	7.02
	6H	7.12	7.12
	7H	7.48	7.46
Gln 40	NH	7.95	8.00
	α-CH	4.30	4.29
	β-CH_2	1.96, 1.82	1.95, 1.80
	γ-CH_2	2.19, 2.12	2.19, 2.12
	ε-NH_2	7.42, 6.80	7.47, 6.86
Pro 41	α-CH	4.22	4.19
	β-CH_2	2.21, 1.82	2.22, 1.95
	γ-CH_2	1.95	1.82
	δ-CH_2	3.48, 3.41	3.48, 3.42
Ala 42	NH	8.17	8.23
	α-CH	4.25	4.23
	β-CH_3	1.42	1.41
Val 43	NH	7.88	7.98
	α-CH	4.00	3.98
	β-CH	2.12	2.10
	γ-CH_3	0.98, 0.94	0.97, 0.92
Gln 44	NH	8.26	8.34
	α-CH	4.22	4.21
	β-CH_2	2.07, 2.02	2.04
	γ-CH_2	2.36	2.35
	ε-NH_2	7.59, 6.85	7.66, 6.93
Ile 45	NH	7.91	8.02
	α-CH	4.13	4.11
	β-CH	1.92	1.90
	γ-CH_3	0.92	0.91
	γ-CH_2	1.51, 1.25	1.51, 1.24
	δ-CH_3	0.88	0.87
Leu 46	NH	8.01	8.11
	α-CH	4.37	4.37
	β-CH_2	1.71, 1.63	1.69
	γ-CH	1.61	1.61
	δ-CH_3	0.93, 0.87	0.92, 0.85
Leu 47	NH	7.55	7.64
	α-CH	4.21	4.18
	β-CH_2	1.61	1.61
	γ-CH	1.59	1.56
	δ-CH_3	0.87	0.89, 0.83

[a] The assignment of diastereotopic atom pairs is not stereospecific.
[b] CCK_A-R(32–47) 1.3 mM, DPC-d_{38} 168 mM, H_2O/D_2O 90%, pH = 6.5. Chemical shifts referenced to external TMS.

optimized conformers. An overlay of 30 optimized structures where the RMSD between the backbone atoms of residues 33–46 and residues 40–46 has been minimized is shown in Figure 1. The average residual target function for these 30 structures was 0.25 Å^2, indicating that the calculated structures were fully consistent with the NOE-derived distance constraints and were sterically consistent. As a matter of fact, there were no interproton distances having consistent violations larger than 0.2 Å

(Table 2). Despite the low target function values, the pairwise backbone and heavy atom RMSD values calculated after best superposition over segment 33–46 in the ensemble of 30 structures showed quite high values for a peptide of this size (backbone and heavy atoms RMSD are 2.03 Å and 2.98 Å, respectively). Thus, the set of geometric constraints derived from NOE measurement was not sufficient

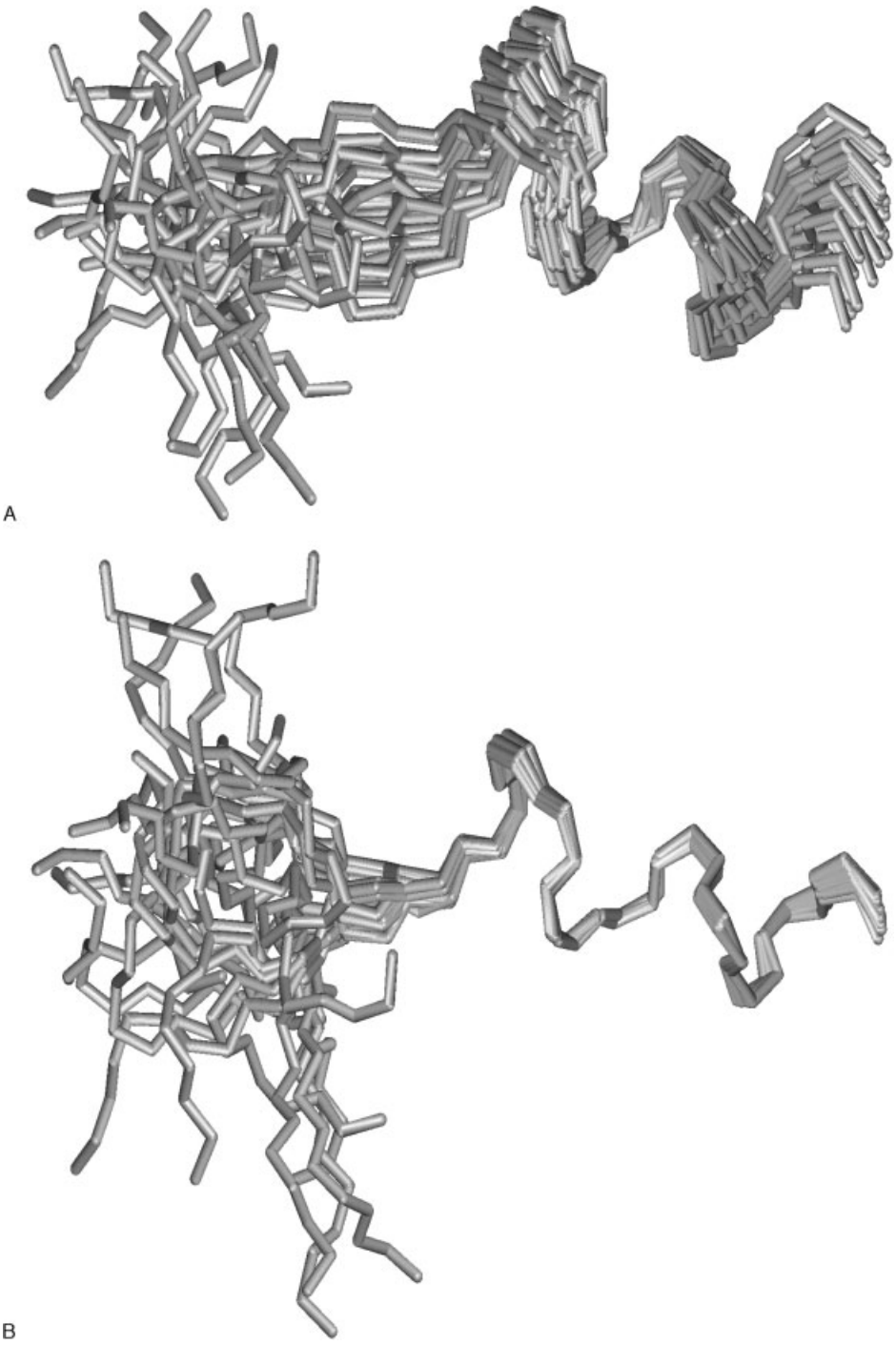

Figure 1 Overlay of 30 structures of CCK_A-R(32–47) obtained by restrained TAD with simulated annealing and energy minimization. The RMSD between the backbone atoms of **(A)** residues 33–46 and **(B)** residues 40–46 has been minimized. The *C*-terminus is on the right.

to achieve a structural model endowed with a high global definition. However, the inspection of RMSDs calculated after best superposition of shorter backbone segments (Table 2) reveals that the structure of CCK_A-R(32–47) is poorly defined in the *N*-terminal region (the backbone RMSD of segment 33–38 has a value of 1.69 Å) but becomes more defined in the central and in the *C*-terminal regions (the backbone RMSD is 0.11 Å for segment 39–45). This finding is not surprising if it is considered that the geometric constraints derived from NOE measurements are not uniformly distributed along the peptide residues, but rather concentrated in the segment 37–47 (only 8 out of 139 constraints were found between atom pairs belonging to segment 32–36). The small structural relevance of NOE constraints observed for the *N*-terminal part of the molecule can be ascribed to conformational averaging processes, which typically produce a marked decrease in NOE peak intensity. To minimize the loss of significant NOE contacts due to conformational averaging, structure optimization was repeated with NOE data acquired at a lower temperature (285 K) and longer mixing time (200 ms). Under these conditions a higher number of constraints involving the protons belonging to segment 32–36 could be obtained (31 out of a total number of 173), but also in this case they were not sufficient to define uniquely the conformation at the *N*-terminus of the peptide. No significant difference in the conformation and definition of segment 40–46 was found between the models obtained from NOE distances measured at 298 and 285 K. The presence of multiple conformations at the *N*-terminus is consistent with the detection (at 285 K) of a double set of signals for residues Gln^{32}, Pro^{33} and Arg^{34}. Thus, it may be concluded that the *N*-terminus of the peptide is endowed with a higher conformational

Table 2 Summary of the NMR Derived Constraints Used for Torsion Angle Dynamics with Simulated Annealing Calculations and Results from Structure Optimization

	DPC/water T = 298 K [a]	DPC/water T = 285 K [b]
Interproton upper distance bounds from NOEs		
Total number	139	173
$i, i+1$	66	62
$i, i+2$	56	85
$i, i+3$	4	10
$i, i+4$	11	12
$i, i+5$ or more	2	4
Structure calculation		
Accepted conformers [c]	30	30
Residual target function ± SD ($Å^2$)[d]	0.25 ± 0.01	0.13 ± 0.02
Violations of upper distance bounds [e]	7	2
Violations of van der Waals lower bounds [e]	2	1
Global RMSD ± sd (Å)		
Segment 33–46, backbone	2.03 ± 0.66	1.46 ± 0.56
Segment 33–46, heavy atoms	2.98 ± 0.68	2.30 ± 0.66
Segment 33–38, backbone	1.69 ± 0.44	0.99 ± 0.34
Segment 33–38, heavy atoms	3.50 ± 0.75	2.41 ± 0.70
Segment 39–45, backbone	0.11 ± 0.07	0.14 ± 0.10
Segment 39–45, heavy atoms	0.69 ± 0.21	0.40 ± 0.18

[a] CCK_A-R(32–47) 1.3 mM, DPC-d_{38} 170 mM, H_2O/D_2O 90%, pH = 6.5, T = 298 K, NOESY mixing time 100 ms.
[b] CCK_A-R(32–47) 1.3 mM, DPC-d_{38} 170 mM, H_2O/D_2O 90%, pH = 6.5, T = 285 K, NOESY mixing time 200 ms.
[c] Selected out of 1000 minimized conformers for structure analysis and statistics.
[d] Averaged over all accepted conformers.
[e] Violations larger than 0.1 Å consistently found in at least one-third of the accepted structures. No violation larger than 0.2 Å was found.

flexibility with respect to the middle and *C*-terminal parts. The instability of regular secondary structure motifs at the *N*-terminus is also consistent with the presence of the Pro residues at positions 33 and 35. Ongoing from the *N*-terminal to the *C*-terminal edge, the structure of CCK_A-R(32–47) becomes more well defined, and the region of the peptide encompassing residues 42–46 is endowed with a defined α-helix conformation. The α-helix shows a tendency to continue (although very distorted) through Pro^{41} up to residue Gln^{44}. In segment 37–39 no regular secondary structure motifs can be identified even though the calculated models are still fairly well defined.

To obtain more insights into the mode of interaction between the peptide and DPC micelles, a titration of the micelle/CCK_A-R(32–47) complex with 5-DS was performed. Under the conditions used for our experiments ([DPC] = 168 mM, $[CCK_A - R(32–47)] = 1.5$ mM, $[5 - DS] = 0.7$ mM), 5-DS was shown to completely insert within DPC micelles without causing an appreciable modification of their structure, each micelle containing no more than one molecule of spin label [32]. Upon addition of 5-DS, an unspecific broadening of the peptide resonances was observed. The line broadening effect can be easily observed in the amide/aromatic region, where spectral overlap is minimum (Figure 2). All the signals of the indole ring of Trp^{39} become broader, indicating that the peptide does interact with the DPC micelles. Intriguingly, the side-chain amide protons of Gln^{32} and Gln^{40} are broadened, whereas those belonging to Gln^{44} are relatively unaffected by 5-DS. The inspection of the aliphatic region of the spectrum indicates that line broadening effects are not regioselective. Therefore no specific portions of the peptide can be identified which come into closer contact with the spin label, which is known to locate approximately at the level of the phosphate headgroups of DPC molecules [32]. No periodicity of line broadening effects along the amino acid sequence could be found, suggesting that CCK_A-R(32–47) does not penetrate the surface of the micelle nor does it assume a fixed orientation with respect to the micelle surface. Rather, the peptide can be envisaged as tumbling on the surface of the micelle and eventually exchanging with the aqueous phase. Consistently, no intermolecular NOEs between the phospholipid moiety and the receptor fragment were detected.

Finally, a titration of CCK_A-R(32–47) in DPC/water with CCK8 was carried out to assess whether a ligand/receptor bimolecular complex did form. The experimental conditions of this titration were the same as those described by Pellegrini and Mierke [6], who reported analogous investigations using CCK_A-R(1–47) instead of CCK_A-R(32–47). No intermolecular NOEs or changes in the chemical shift of Trp^{39} in CCK_A-R(32–47) were detected, up to a ligand/receptor ratio of 3 : 1. Thus, no direct evidence of any specific interaction between the receptor fragment and CCK8 could be found in the case of CCK_A-R(32–47).

Fluorescence and CD Studies

As for CCK_A-R(1–47) [6,7], binding experiments were performed in the presence of micellar concentrations of surfactant agents. In this regard, we showed that CCK_A-R(1–47) undergoes concomitant secondary and tertiary structural rearrangements at SDS concentrations just preceding the detergent c.m.c. [7]. This was interpreted as evidence that the peptide interacts with SDS micelles rather than with SDS monomer units. On this basis, we investigated the onset of SDS-induced modifications of CCK_A-R(32–47). Figure 3 shows that cooperative transitions monitored by CD (sensitive to secondary structure modification) and shift of the wavelength of maximum emission (sensitive to overall structural rearrangements) overlap. Indeed, differences in the slope of the two curves are negligible and transition midpoints are centred at 1.91 ± 0.07 and 1.86 ± 0.10 mM SDS for dichroic activity at 220 nm and the shift of the fluorescence emission is maximum, respectively. However, it is worth noting that in neither case do these structural transitions superimpose to those previously obtained for CCK_A-R(1–47), which are also reported to show a direct comparison (midpoints at 3.28 ± 0.08 and 3.11 ± 0.06 mM SDS, for CD and fluorescence, respectively). SDS binding to CCK_A-R(32–47) takes place ~1.3 concentration units (mM) below the detergent c.m.c. On the hypothesis that co-micellization of CCK_A-R(1–47) with SDS is the molecular mechanism that drives the binding interaction of this peptide with CCK8, it is likely that monomeric SDS could modify the structure of CCK_A-R(32–47) so as to lead to a biologically inactive conformation and to prevent proper interaction with the micellar (membrane-like) environment.

When DPC was used instead of SDS to create a membrane-mimicking environment, a very different behaviour was observed. The fluorescence emission maximum of CCK_A-R(32–47) was not modified upon addition of DPC to the buffer solution (Table 3)

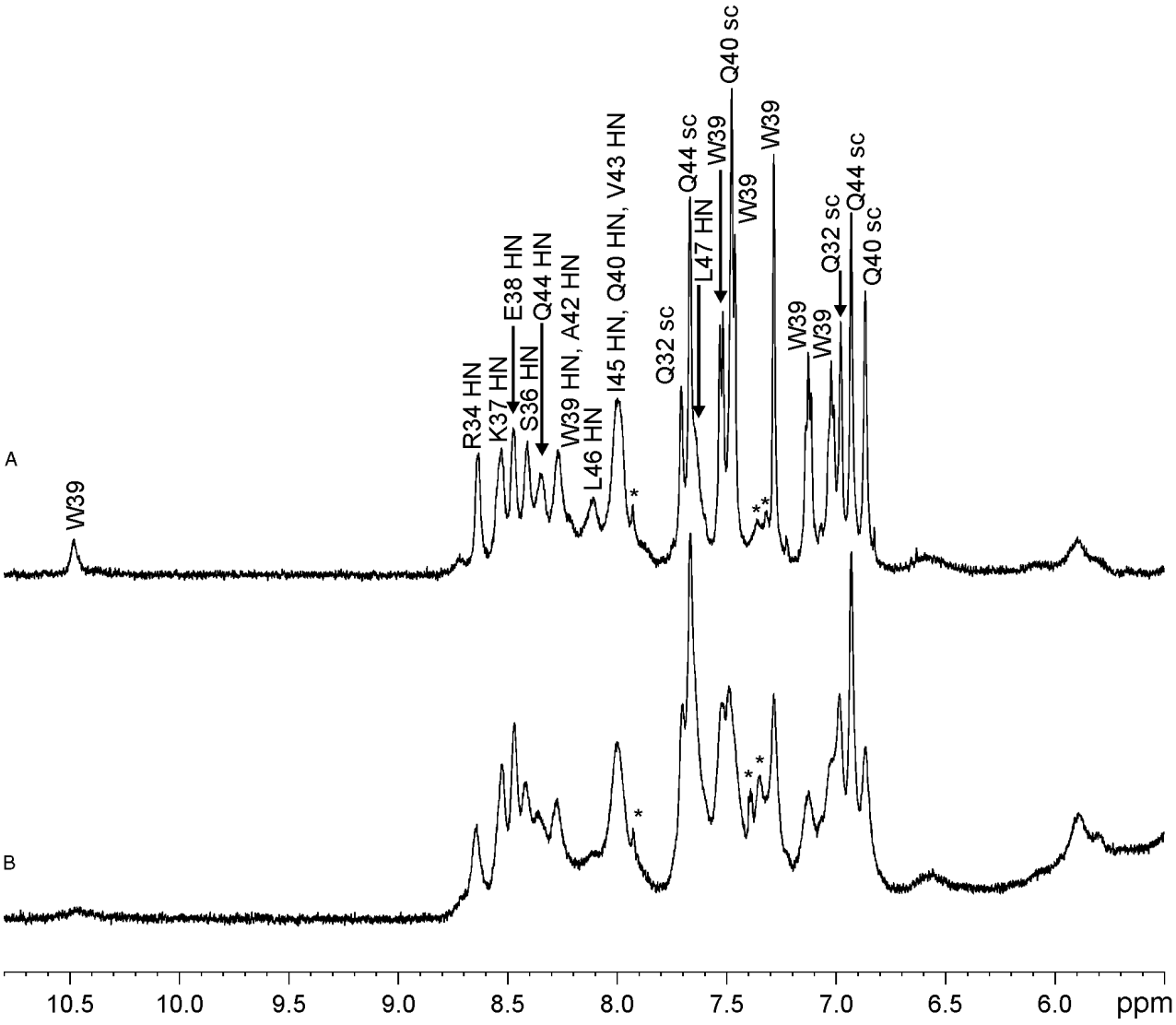

Figure 2 ^{1}H-NMR spectra (amide/aromatic region) of CCK_A-R(32–47) in DPC/water (1.3 mM, DPC-d_{38} 168 mM, H_2O/D_2O 90%, pH = 6.5, T = 285 K) **(A)** before and **(B)** after addition of 5-doxylstearate (final concentration 0.7 mM). The Y-scale of the spectrum in **(B)** has been expanded with respect to **(A)**. The assignment of the peptide resonances is shown. Asterisks denote impurities. Note the broadening of the resonances of Trp^{39} in the presence of 5-doxylstearate.

either at submicellar or micellar concentrations. This indicates that the interaction between CCK_A-R(32–47) and DPC micelles, if any, may not be detected by fluorescence. However, the finding that CCK_A-R(1–47) and CCK_A-R(32–47) interact with the DPC or SDS micelles in different ways is not sufficient by itself to infer that CCK_A-R(32–47) cannot bind CCK8, because it is the membrane-associated conformation of CCK8 that first interacts and is recognized by the receptor [33]. On this point, Table 3 clarifies that the addition of micellar concentrations of either SDS or DPC shifts the emission maximum of CCK8 from ~352 nm to ~342 nm. In either case this blue shift is associated with a functionally significant structural modification [6,7]. Therefore, several CCK8 titrations were performed, using different CCK_A-R(32–47) concentrations in the presence of both submicellar and micellar amounts of either SDS or DPC. The results of a typical experiment are shown in Figure 4, which confirm that the behaviour of CCK_A-R(32–47) is different from that previously observed for CCK_A-R(1–47). In fact, after subtraction of the individual signals of the two non-interacting

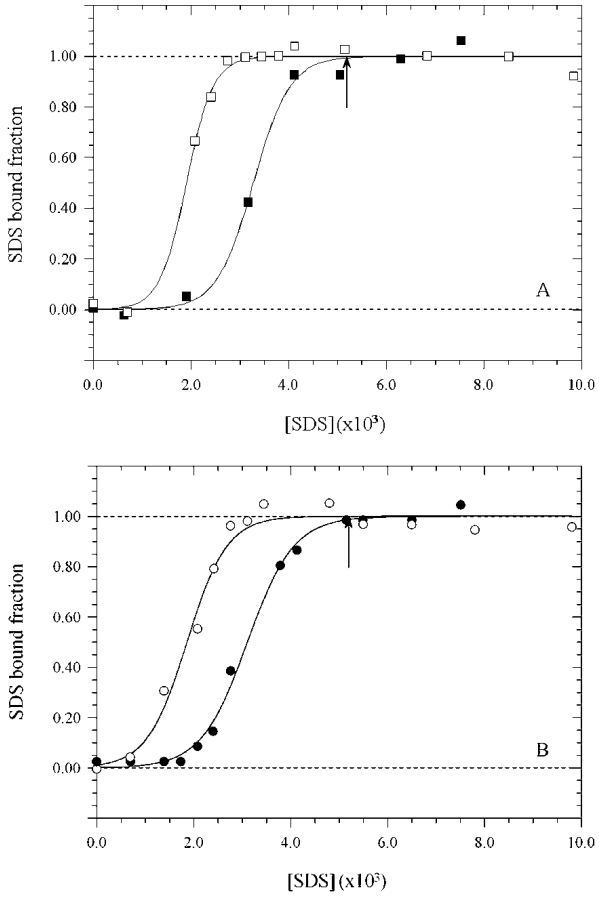

Figure 3 Titration with SDS. **(A)** Circular dichroism. Ellipticity changes at 220 nm covered the range from −3800 to −5700 deg cm^2 dmol^{-1} and from −3500 to −6000 deg cm^2 dmol^{-1} for CCK_A-R(32–47) (□) and CCK_A-R(1–47) (■), respectively, on a per residue basis. **(B)** Fluorescence. The emission maximum was shifted from 354 to 344 nm and from 352 to 335 nm for CCK_A-R(32–47) (○) and CCK_A-R(1–47) (●), respectively. The arrows indicate the c.m.c. of SDS, as obtained by different techniques under conditions similar to those of our experiments (10 mM phosphate buffer, pH 7.2) [26–28].

Table 3 Maximum Emission Wavelength of Peptides (nm)

	10 mM buffer, pH 7.2	2 mM DPC	8 mM SDS
CCK_A-R(1–47)	352	N.D.	335
CCK_A-R(32–47)	354	354	344
CCK8	352	342	342

species, no hyperbolic diminution of the residual fluorescence could be detected for CCK_A-R(32–47)

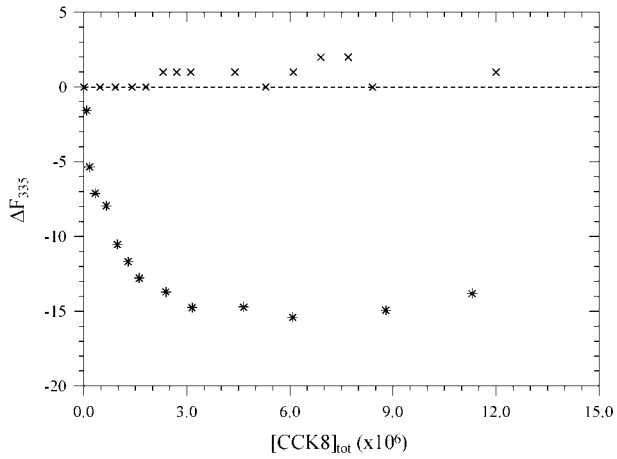

Figure 4 Titration with CCK8. Fluorescence modification on addition of small aliquots of CCK8 from a concentrated solution to CCK_A-R(32–47) (×) and CCK_A-R(1–47) (*), respectively, in the presence of detergent concentration close to the c.m.c. in water (8.3 or 1.5 mM for SDS [26–28] or DPC [29], respectively). The ordinate represents the residual fluorescence signal at 335 nm after subtraction of the individual contributions of peptide and CCK8. The hyperbolic trend of the CCK_A-R(1–47) data points reflects binding, with a dissociation constant of about 250 nM [7]. The fluorescence signal does not change for CCK_A-R(32–47), suggesting that binding does not take place.

compared with CCK_A-R(1–47). This provides some, but not conclusive, evidence that binding to CCK8 may be absent. In any case, this indirectly suggests that each receptor-derived peptide interacts with surfactant differently. It seems then plausible that the binding ability of CCK_A-R(1–47) depends on the proper insertion into a membrane-like environment.

DISCUSSION

In the presence of micellar concentrations of surfactant agents the titration of CCK_A-R(32–47) with CCK8 followed by NMR and fluorescence techniques gave no evidence of a specific ligand binding interaction. Instead, a dissociation constant of about 250 nM was estimated for CCK_A-R(1–47) in SDS [7] and direct evidence for the formation of a bimolecular complex between CCK_A-R(1–47) and CCK8 was obtained in DPC [6]. The different affinities for the ligand shown by CCK_A-R(32–47) and CCK_A-R(1–47) are paralleled by the fact that the two receptor fragments interact with micelles in very different ways. CCK_A-R(1–47) strongly interacts

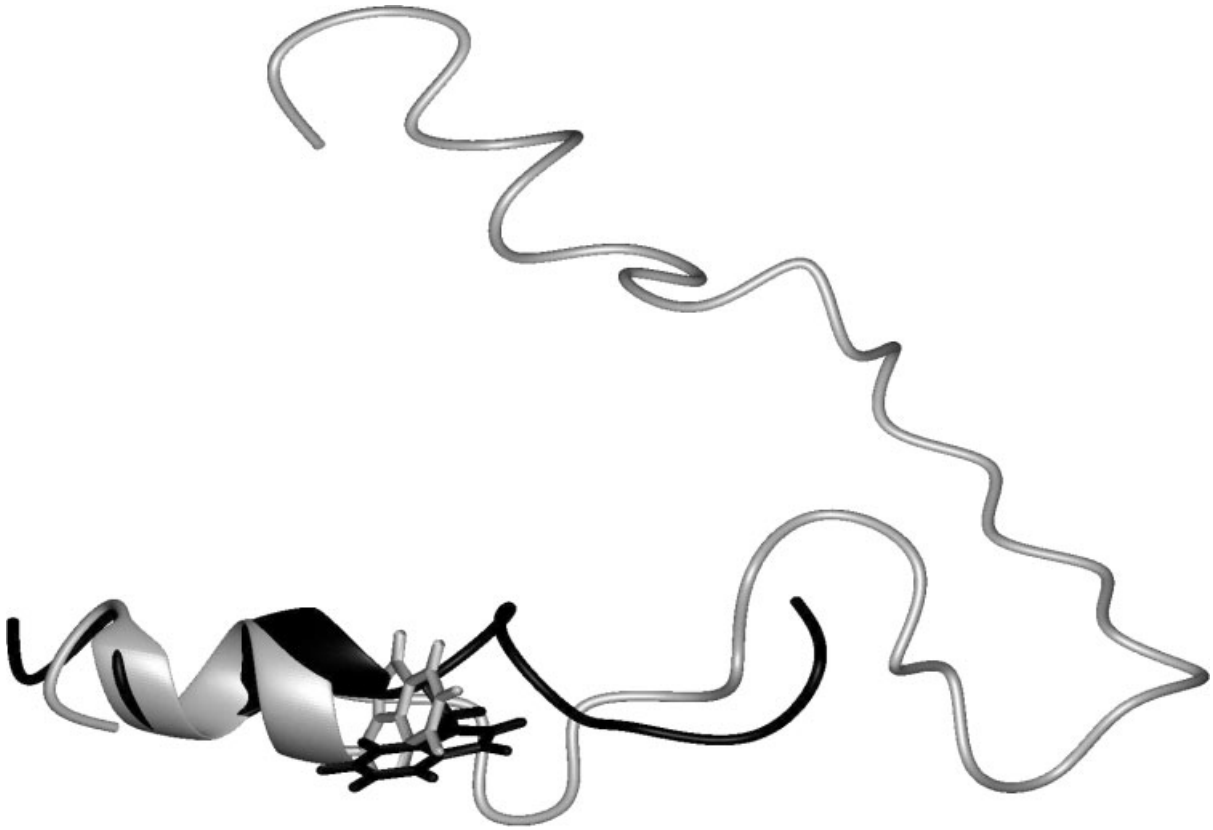

Figure 5 Overlay of a representative structure of CCK_A-R(32–47) (dark colour) with a representative structure of CCK_A-R(1–47) (light colour) obtained by NMR in DPC/water solution (both structures shown as ribbon plots). The molecular model of CCK_A-R(1–47) was retrieved from the Protein Data Bank (PDB accession number 1D6G, after Pellegrini and Mierke [6]). The RMSD between the backbone atoms of residues 40–46 has been minimized. The Trp^{39} side chains are also shown.

with either DPC and SDS at surfactant concentrations close to the c.m.c. On the other hand, CCK_A-R(32–47) interacts with SDS at a surfactant concentration well below the c.m.c., whereas it only weakly interacts with DPC (both at micellar and submicellar concentrations). It may be envisaged that the mode of interaction between the receptor segments and the membrane mimicking environment plays a major role towards the stabilization of the receptor biologically active conformation. Further insights into the relationship between receptor/micelle interaction and bioactive conformation can be gained by comparing the NMR structures of CCK_A-R(32–47) and CCK_A-R(1–47) in DPC. The structure of DPC micelle-bound CCK_A-R(1–47) was determined by Pellegrini and Mierke [6], who also characterized the bimolecular complex between the receptor and CCK8. This study pointed out that the ligand/receptor contact site is located around residue Trp^{39} of CCK_A-R(1–47), and that the receptor segment in the bimolecular complex adopts a well defined orientation with respect to the micelle. Figure 5 shows an overlay of CCK_A-R(32–47) and CCK_A-R(1–47) solution structures where the backbone RMSD over segment 40–46 has been minimized. The regions encompassing residues 40–46 of both receptor segments share a substantially similar secondary structure, with the *C*-terminal segments (residues 42–45) having the highest conformational similarity (α-helix structure). On going from the *C*-terminus to the *N*-terminus, the structures start to significantly diverge at the level of residue Trp^{39}. This fact is very interesting, since Trp^{39} has a key role in the ligand binding interaction. Beyond Trp^{39} (segment 33–38), the backbone conformation of CCK_A-R(32–47) becomes poorly defined because of flexibility, whereas in CCK_A-R(1–47) the backbone conformation is stabilized by a β-sheet structure and by the presence of a disulfide bridge between

Cys^{18} and Cys^{29}. Experiments with 5-DS confirm that CCK_A-R(32–47) does not assume a fixed orientation with respect to the DPC micelle, and that it rather tumbles on the surface of the micelle and/or exchanges with the aqueous phase. On the other hand, the relative orientation between CCK_A-R(1–47) and DPC micelles is more defined, since a specific line broadening effect induced by the spin label was observed for the *C*-terminal and the *N*-terminal α-helix domains [6]. The central portions of the molecule are less affected by the spin label, and presumably project towards the solvent. Thus, it can be concluded that CCK_A-R(32–47) can not maintain the biologically active conformation because of the lack of stabilizing tertiary structure interactions (including the disulfide bridge) and because of the lack of proper contacts with the DPC micelle surface.

Also when SDS is used as the surfactant, instead of DPC, there is a significant difference in the interaction of CCK_A-R(1–47) and CCK_A-R(32–47) with micelles. SDS-induced rearrangements of CCK_A-R(1–47) ended at ~5 mM SDS, which coincides with the c.m.c. at the ionic strength of experiments, being lower that the c.m.c. in pure water (~8 mM) [26–28]. Since above the c.m.c. any ionic surfactant is incorporated into micelles with an inverse ionic strength dependence [30,31], it can be inferred that CCK_A-R(1–47) co-micellizes with SDS. The addition of SDS to CCK_A-R(32–47) also resulted in sigmoidal modifications of both the maximum emission wavelength (sensitive to overall structural rearrangements) and the dichroic activity at 220 nm (sensitive to secondary structure modification), but these structural transitions took place at a detergent concentration below the c.m.c. Thus, it can be envisaged that CCK_A-R(32–47) and SDS form non-micellar adducts which prevent the onset of a functionally significant interaction between the receptor segment and detergent *via* micelle formation. In this view, segment 1–31 takes the role to drive the interaction between the *N*-terminal receptor segment and SDS, thus allowing for the proper positioning of the receptor *N*-terminal tail on the micelle surface.

Acknowledgements

This work was supported by grants from Italian MURST (PS Oncologia) and from the Company Bracco Imaging SpA, Milan, Italy.

REFERENCES

1. Kennedy K, Gigoux V, Escrieut C, Maigret B, Martinez J, Moroder L, Frehel D, Gully D, Vaysse N, Fourmy D. Identification of two amino acids of the human cholecystokinin-A receptor that interact with the *N*-terminal moiety of cholecystokinin. *J. Biol. Chem.* 1997; **272**: 2920–2926.
2. Gigioux V, Maigret B, Escrieut C, Silvente-Poirot S, Bouisson M, Fehrentz J, Moroder L, Gully D, Martinez J, Vaysse N, Fourmy D. Arginine 197 of the cholecystokinin-A receptor binding site interacts with the sulfate of the peptide agonist cholecystokinin. *Protein Sci.* 1999; **8**: 2347–2354.
3. Ji Z, Hadac EM, Henne RM, Patel SA, Lybrand TP, Miller LJ. Direct identification of a distinct site of interaction between the carboxyl-terminal residue of cholecystokinin and the type A cholecystokinin receptor using photoaffinity labeling. *J. Biol. Chem.* 1997; **272**: 24 393–24 401.
4. Ding X, Dolu V, Hadac EM, Holicky EL, Pinon DI, Lybrand TP, Miller LJ. Refinement of the structure of the ligand-occupied cholecystokinin receptor using a photolabile amino-terminal probe. *J. Biol. Chem.* 2001; **276**: 4236–4244.
5. Giragossian C, Mierke DF. Intermolecular interactions between cholecystokinin-8 and the third extracellular loop of the cholecystokinin-2 receptor. *Biochemistry* 2001; **40**: 3804–3809.
6. Pellegrini M, Mierke DF. Molecular complex of the cholecystokinin-8 *N*-terminus of the cholecystokinin-A receptor by NMR spectroscopy. *Biochemistry* 1999; **38**: 14 775–14 783.
7. Ragone R, De Luca S, Tesauro D, Pedone C, Morelli G. Fluorescence studies on the binding between 1–47 fragment of the cholecystokinin receptor CCKA-R(1–47) and nonsulfated cholecystokinin octapeptide CCK8. *Biopolymers* 2001; **56**: 47–53.
8. Silvente-Poirot S, Escrieut C, Wank SA. Role of the extracellular domains of the cholecystokinin receptor in agonist binding. *Mol. Pharmacol.* 1998; **54**: 364–371.
9. Coste J, Le-Nguyen D, Castro B. PyBOP: A new peptide coupling reagent devoid of toxic byproduct. *Tetrahedron Lett.* 1990; **31**: 205–208.
10. Albericio F, Carpino LA. In *Methods in Enzymology*. Academic Press: London, 1997; **289**: 104.
11. Edelhoch H. Spectroscopic determination of tryptophan and tyrosine in proteins. *Biochemistry* 1967; **6**: 1948–1954.
12. Pace CN, Vajdos F, Fee L, Grimsley G, Gray T. How to measure and predict the molar absorption coefficient of a protein. *Protein Sci.* 1995; **4**: 2411–2423.
13. Piotto M, Saudek V, Sklenar V. Gradient-tailored excitation for single-quantum NMR spectroscopy of aqueous solutions. *J. Biomol. NMR* 1992; **2**: 661–666.

14. Sklenar V, Piotto M, Leppik R, Saudek V. Gradient-tailored water suppression for ^{1}H-^{15}N HSQC experiments optimized to retain full sensitivity. *J. Magn. Reson.* 1993; **A102**: 241–245.
15. Braunschweiler L, Ernst RR. Coherence transfer by isotropic mixing: application to proton correlation spectroscopy. *J. Magn. Reson.* 1983; **53**: 521–528.
16. Bax A, Davis DG. MLEV-17 based two-dimensional homonuclear magnetization transfer spectroscopy. *J. Magn. Reson.* 1985; **65**: 355–360.
17. Jeener J, Meier BH, Bachmann P, Ernst RR. Investigation of exchange processes by two-dimensional NMR spectroscopy. *J. Chem. Phys.* 1979; **71**: 4546–4553.
18. Piantini U, Sørensen OW, Ernst RR. Multiple quantum filters for elucidating NMR coupling networks. *J. Am. Chem. Soc.* 1982; **104**: 6800–6801.
19. John BK, Plant D, Webb P, Hurd RE. Effective combination of gradients and crafted RF pulses for water suppression in biological samples. *J. Magn. Reson.* 1992; **98**: 200–206.
20. Bartels C, Xia TH, Billeter M, Güntert P, Wüthrich K. The program XEASY for computer-supported NMR spectral analysis of biological macromolecules. *J. Biomol. NMR* 1995; **6**: 1–10.
21. Wüthrich K. In *NMR of Proteins and Nucleic Acids*. Wiley: New York, 1986.
22. Güntert P, Mumenthaler C, Wüthrich K. Torsion angle dynamics for NMR structure calculation with the new program DYANA. *J. Mol. Biol.* 1997; **273**: 283–298.
23. Güntert P, Braun W, Wüthrich K. Efficient computation of three-dimensional protein structures in solution from nuclear magnetic resonance data using the program DIANA and the supporting programs CALIBA, HABAS and GLOMSA. *J. Mol. Biol.* 1991; **217**: 517–530.
24. Koradi R, Billeter M, Wüthrich K. MOLMOL: a program for display and analysis of macromolecular structures. *J. Mol. Graphics* 1996; **14**: 51–55.
25. Némethy G, Pottle MS, Scheraga HA. Energy parameters in polypeptides. IX. Updating of geometric parameters, nonbonded interactions and hydrogen bond interactions for the naturally occurring amino acid. *J. Phys. Chem.* 1983; **87**: 1883–1887.
26. Emerson MF, Holtzer A. On the ionic strength dependence of micelle number. *J. Phys. Chem.* 1965; **69**: 3718–3721.
27. Emerson MF, Holtzer A. On the ionic strength dependence of micelle number. II. *J. Phys. Chem.* 1967; **71**: 1898–1907.
28. Esposito C, Colicchio P, Facchiano A, Ragone R. Effect of a weak electrolyte on the critical micellar concentration of sodium dodecyl sulfate. *J. Colloid Interface Sci.* 1998; **200**: 310–312.
29. Kleinschmidt JH, Wiener MC, Tamm LK. Outer membrane protein A of *E. coli* folds into detergent micelles, but not in the presence of monomeric detergent. *Protein Sci.* 1999; **8**: 2065–2071.
30. Kresheck GC. In *Water: A Comprehensive Treatise*, Vol. 4, Franks F (ed.). Plenum: New York, 1975; 95–167.
31. Ambrosone L, Ragone R. The interaction of micelles with added species and its similarity to the denaturant binding model of proteins. *J. Colloid Interface Sci.* 1998; **205**: 454–458.
32. Brown LR, Bösch C, Wüthrich K. Location and orientation relative to the micelle surface for glucagon in mixed micelles with dodecylphosphocholine. EPR and NMR studies. *Biochim. Biophys. Acta* 1981; **642**: 296–312.
33. Moroder L. On the mechanism of hormone recognition and binding by the CCK-B/gastrin receptor. *J. Pept. Sci.* 1997; **3**: 1–14.

